processes

MDPI

*Article*

# Study on the Interaction Propagation Mechanism of Inter-Cluster Fractures under Different Fracturing Sequences

**Xiaojun Cai [1], Weixuan Zhao [1], Tianbao Hu [1], Xinwei Du [1], Haiyang Wang [2,*] and Xiong Liu [2]**

[1] Changqing Oilfield Company, China National Petroleum Corporation, Xi'an 710065, China; 23211010043@stumail.xsyu.edu.cn (X.C.); 23212010116@stumail.xsyu.edu.cn (W.Z.); 23212010094@stumail.xsyu.edu.cn (T.H.); 21211010056@stumail.xsyu.edu.cn (X.D.)
[2] School of Petroleum Engineering, Xi'an Shiyou University, Xi'an 710065, China; liuxiong2016@xsyu.edu.cn
* Correspondence: wanghaiyang@xsyu.edu.cn

**Abstract:** Horizontal-well multi-cluster fracturing is one of the most important techniques for increasing the recovery rate in unconventional oil and gas reservoir development. However, under the influence of complex induced stress fields, the mechanism of interaction and propagation of fractures within each segment remains unclear. In this study, based on rock fracture criteria, combined with the boundary element displacement discontinuity method, a two-dimensional numerical simulation model of hydraulic fracturing crack propagation in a planar plane was established. Using this model, the interaction and propagation process of inter-cluster fractures under different fracturing sequences within horizontal well segments and the mechanism of induced stress field effects were analyzed. The influence mechanism of cluster spacing, fracture design length, and fracture internal pressure on the propagation morphology of inter-cluster fractures was also investigated. The research results indicate that, when using the alternating fracturing method, it is advisable to appropriately increase the cluster spacing to weaken the inhibitory effect of induced stress around the fractures created by prior fracturing on subsequent fracturing. Compared to the alternating fracturing method, the propagation morphology of fractures under the symmetrical fracturing method is more complex. At smaller cluster spacing, fractures created by prior fracturing are more susceptible to being captured by fractures from subsequent fracturing. The findings of this study provide reliable theoretical support for the optimization design of fracturing sequences and fracturing processes in horizontal well segments.

**Keywords:** horizontal-well staged multi-cluster fracturing; fracture propagation; induced stress field; numerical simulation; displacement discontinuity method



**Citation:** Cai, X.; Zhao, W.; Hu, T.; Du, X.; Wang, H.; Liu, X. Study on the Interaction Propagation Mechanism of Inter-Cluster Fractures under Different Fracturing Sequences. *Processes* **2024**, *12*, 971. https://doi.org/10.3390/pr12050971

Academic Editor: Carlos Sierra Fernández

Received: 25 April 2024
Revised: 7 May 2024
Accepted: 7 May 2024
Published: 10 May 2024



## 1. Introduction

Multi-cluster fracturing technology in horizontal wells is a revolutionary method for oil and gas extraction, combining the advantages of horizontal drilling and fracturing techniques [1,2]. In traditional vertical drilling, oil and gas extraction primarily relies on the natural permeability of underground rock formations, often limiting production rates. However, multi-cluster fracturing technology in horizontal wells involves drilling horizontal segments in the subsurface and injecting high-pressure fluids, inducing rock fracturing to create extensive fractures and release additional hydrocarbons, thereby significantly enhancing extraction efficiency [3].

The key to the multi-cluster fracturing technology in horizontal wells lies in dividing the horizontal well into different fracturing stages, each subdivided into multiple fracturing clusters. By conducting independent fracturing operations within each cluster, better coverage of the underground rock formations is achieved, maximizing the release of hydrocarbon resources from the reservoir [4]. Through staged fracturing, engineers can optimize fracturing designs based on geological conditions, rock properties, and fluid dynamics, thus maximizing the release of hydrocarbon resources from underground reservoirs [5]. The advantages of multi-cluster fracturing technology in horizontal wells include the following [6,7]: (1) By deploying multiple fracturing clusters across various segments of the horizontal well, a more uniform coverage of the underground reservoir is achieved, enhancing oil and gas recovery rates and extraction efficiency, while avoiding uneven production within the fracturing zone. (2) Precise fracturing designs can be tailored based on geological features and rock properties, ensuring more effective fracturing outcomes for each cluster. (3) Despite the additional construction costs associated with deploying multiple clusters, the increase in recovery rates and extraction efficiency can lower the production costs per unit of oil and gas, thereby enhancing the project's economic benefits. Horizontal-well staged fracturing technology holds significant importance for optimizing oil and gas resource extraction, reducing environmental impacts, and improving economic benefits. With the continuous growth in energy demand and the depletion of oil and gas resources, this technology will continue to play a crucial role in the oil and gas industry, promoting sustainable energy development and economic prosperity [8,9].

Extensive experimental and numerical simulation studies have been conducted on the multi-cluster fracturing technology in horizontal wells. Researchers have explored the effects of various fracturing parameters (such as fracturing fluid type, injection rate, fracturing pressure, etc.) on fracturing outcomes through experiments and numerical simulations to optimize fracturing construction schemes and enhance oil and gas production capacity [10–14]. Some studies have focused on the distribution of fluids in the reservoir and their influence on the formation of hydraulic fracture networks. They have investigated different fluid injection strategies through experiments and numerical simulations to maximize the control volume of fracture networks in the reservoir [15–19]. Researchers have also conducted in-depth studies on the mechanical response of formations, including the formation, propagation, and closure mechanisms of formation fractures. They have simulated the mechanical behavior of formations through numerical simulations and compared the results with experiments to better understand the mechanical response patterns of formations [20–22]. In order to more accurately simulate the process of multi-cluster fracturing in horizontal wells, researchers have also carried out multi-physics field coupling simulations, including coupling simulations of formation mechanics, fluid transport, and chemical reactions, to comprehensively evaluate fracturing effects and formation responses [23–26]. These research advancements provide important theoretical guidance and technical support for the engineering application of multi-cluster fracturing technology in horizontal wells. However, there is still limited research on the interaction and propagation mechanisms of inter-cluster fractures within horizontal well segments. It remains unclear how to optimize the fracturing sequence and fracturing construction parameters for each cluster within segments to optimize fracture morphology. Further exploration is needed to understand the influence mechanisms of induced stress field evolution on inter-cluster fracture propagation.

To address the aforementioned issues, this study first established a two-dimensional numerical simulation model for hydraulic fracturing crack propagation based on the boundary element method combined with linear elasticity theory and rock fracture mechanics theory. Subsequently, utilizing this model, we simulated and analyzed the interaction and propagation morphology of multi-cluster fractures within segments under two different fracturing sequences, along with the distribution of induced stress fields. Finally, we delved into the influence mechanisms of cluster spacing, fracture internal pressure, and fracture design length on the interaction and propagation of inter-cluster fractures. Our research provides reliable theoretical support and valuable insights for optimizing the design of construction schemes for multi-cluster fracturing in horizontal well segments.

## 2. Numerical Model Establishment

### 2.1. Basic Principles and Governing Equations

The displacement discontinuity method is a numerical technique for simulating discontinuous problems (such as cracks and joints). The boundary element method (BEM) presents distinct advantages for solving rock fracture mechanics problems. One notable advantage is its ability to directly model the interaction of fractures with surrounding rock boundaries, which is crucial for accurately capturing stress distributions and fracture propagation paths. Unlike finite element methods that require volumetric discretization, BEM focuses solely on the boundaries, significantly reducing computational overhead for large-scale problems. This method naturally accommodates unbounded domains by leveraging fundamental solutions or far-field approximations, thus simplifying the treatment of infinite boundaries such as those encountered in geomechanical contexts.

Based on the boundary element concept, it treats the relative displacement on crack surfaces as the unknowns, transforming the problem into solving a series of linear or nonlinear equations. By solving these governing equations (such as equilibrium equations and boundary conditions), it derives the stress and displacement fields during the crack propagation process [27]. Crouch proposed discretizing elements in an infinite elastic body to simulate the discontinuous distribution of crack displacement [28]. As shown in Figure 1, within an infinite formation, there exists a crack element with a length of 2a. The upper and lower surfaces of the crack are denoted as $y = 0_+$ and $y = 0_-$, respectively. The application of external loads causes changes in relative displacement between the upper and lower surfaces, resulting in tangential displacement variation, represented by $D_x$ (crack shear slip), and normal displacement variation, represented by $D_y$ (crack width).

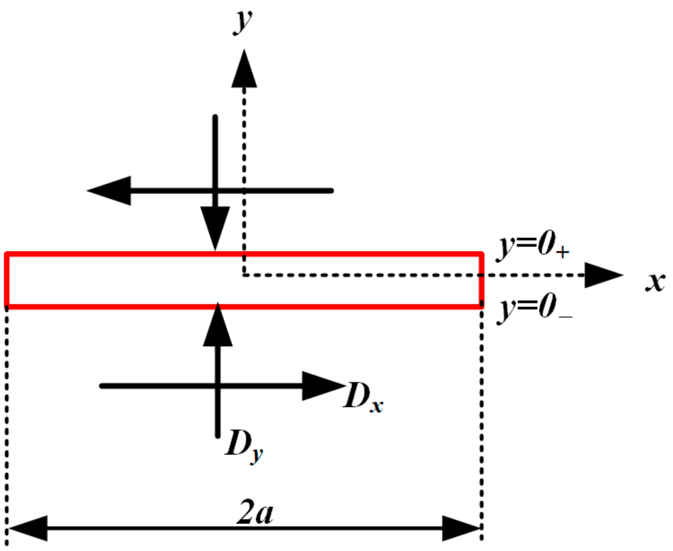


**Figure 1.** Constant displacement discontinuity of crack surface [29].

The displacement difference between the upper and lower surfaces is defined as the displacement discontinuity, and the expression is as follows:

$$\begin{cases} D_x = u_x(x, 0_-) - u_x(x, 0_+) \\ D_y = u_y(y, 0_-) - u_y(y, 0_+) \end{cases} \quad (1)$$

where $u_x$ and $u_y$ represent the displacement along the $x$ and $y$ directions. The positive sign, "+", represents the upper surface of the crack unit, and the negative sign, "−", represents the lower upper surface of the crack unit.

The stress and displacement components generated by the relative displacement ($D_x$ and $D_y$) of the crack unit at any point, $i$, in the plane are as follows:

$$\begin{cases} u_x = D_x\left[2(1-\nu)f_{,y} - yf_{,xx}\right] + D_y\left[-(1-2\nu)f_{,x} - yf_{,xy}\right] \\ u_y = D_x\left[2(1-\nu)f_{,x} - yf_{,xy}\right] + D_y\left[2(1-\nu)f_{,y} - yf_{,yy}\right] \\ \sigma_{xx} = 2GD_x\left(2f_{,xy} + yf_{,xyy}\right) + 2GD_y\left(f_{,yy} + yf_{,yyy}\right) \\ \sigma_{yy} = 2GD_x\left(-yf_{,xyy}\right) + 2GD_y\left(f_{,yy} + yf_{,yyy}\right) \\ \sigma_{xy} = 2GD_x\left(f_{,yy} + yf_{,xyy}\right) + 2GD_y\left(-yf_{,yyy}\right) \end{cases} \tag{2}$$

where $f(x,y)$ is as follows:

$$\begin{aligned} &f(x,y) = -\tfrac{1}{4\pi(1-\nu)}\left[y\left(arctg\tfrac{y}{x-a} - arctg\tfrac{y}{x+a}\right)\right] \\ &-(x-a)\ln\left[(x-a)^2+y^2\right]^{\frac{1}{2}} + (x+a)\ln\left[(x+a)^2+y^2\right]^{1/2} \end{aligned} \tag{3}$$

In the formula, $\sigma_{xx}$ and $\sigma_{yy}$ represent the normal stress along the $x$ and $y$ directions; $\sigma_{xy}$ represents the shear stress; $\nu$ represents Poisson's ratio; $G$ represents the shear modulus; $f(x,y)$ represents the constant displacement discontinuity problem; and $f_{,x}$ and $f_{,y}$, respectively, represent the first-order partial derivatives of $f(x,y)$ with respect to $x$ and $y$, and so on for the remaining multi-order partial derivatives.

For an independent curved crack problem in a plane, when performing the numerical simulation, the curve can be discretized into N small segments connected end to end, that is, N boundary elements (a straight line is used to replace the curve for each element). At this time, the tangential and normal local coordinates s-n of a boundary element, $j$, are shown in Figure 2.

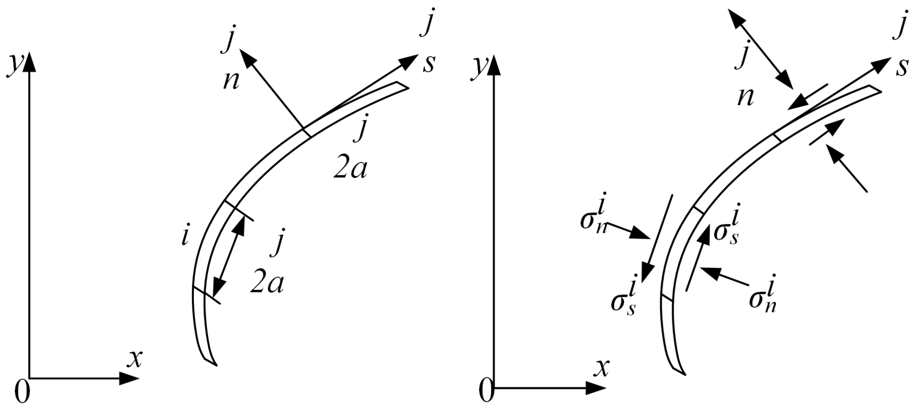


(**a**) (**b**)

**Figure 2.** (**a**) Crack element discretization. (**b**): Stress components in global coordinates $x$-$y$ and local coordinates s-n [29,30].

Coordinate transformation is required when calculating the influence coefficient of discrete element $j$ on discrete element $i$. Usually, the coordinates of element $i$ in the global coordinate system $x$-$y$ need to be transformed into the local coordinate system $s^j$-$n^j$ for calculation. The expression is as follows:

$$\begin{cases} \overline{x_i} = \left(x^i - x^j\right)\cos\beta^j + \left(y^i - y^j\right)\sin\beta^j \\ \overline{y_i} = -\left(x^i - x^j\right)\sin\beta^j + \left(y^i - y^j\right)\cos\beta^j \; i,j = 1,2,3..N \\ \gamma = \beta^i - \beta^j \end{cases} \tag{4}$$

where $x^i$,$x^j$, $y^i$, and $y^j$ represent the coordinates of the midpoints of discrete fracture units $i$ and $j$ in the $x$-$y$ coordinate system; $\beta^i$ and $\beta^j$ represent the angles between the local coordinate systems of discrete fracture units $i$ and $j$ and the global coordinate system $x$-$y$; and $\overline{x_i}$ and $\overline{y_i}$ represent the coordinates of the midpoint of discrete fracture unit $i$ in the local coordinate system s-n.

If the interior of the crack is acted upon by compressive stress, the displacement discontinuity produced on the upper and lower surfaces of unit $j$ is as follows:

$$\begin{cases} \overset{j}{D}_s = \overset{j}{u}{}_s^- - \overset{j}{u}{}_s^+ \\ \overset{j}{D}_n = \overset{j}{u}{}_n^- - \overset{j}{u}{}_n^+ \end{cases} \tag{5}$$

where $\overset{j}{D}_s$ and $\overset{j}{D}_n$ represent the displacement discontinuities of unit body $j$ in the $s$ and $n$ directions; and $\overset{j}{u}_s$ and $\overset{j}{u}_n$ represent the displacement of unit body $j$ in the $s$ and $n$ directions. If the crack unit $j$ has a displacement discontinuity, the stress and displacement components generated at any crack unit $i$ are as follows:

$$\begin{cases} \overset{i}{\sigma}_s = \overset{j,i}{A}_{ss}\overset{j}{D}_s + \overset{j,i}{A}_{sn}\overset{j}{D}_n \\ \overset{i}{\sigma}_n = \overset{j,i}{A}_{ns}\overset{j}{D}_s + \overset{j,i}{A}_{nn}\overset{j}{D}_n \\ \overset{i}{\sigma}_t = \overset{j,i}{A}_{ts}\overset{j}{D}_s + \overset{j,i}{A}_{tn}\overset{j}{D}_n \\ \overset{i}{u}_s = \overset{j,i}{B}_{ss}\overset{j}{D}_s + \overset{j,i}{B}_{sn}\overset{j}{D}_n \\ \overset{i}{u}_n = \overset{j,i}{B}_{ns}\overset{j}{D}_s + \overset{j,i}{B}_{nn}\overset{j}{D}_n \end{cases} \tag{6}$$

where $\overset{i}{\sigma}_s$, $\overset{i}{\sigma}_n$, and $\overset{i}{\sigma}_t$ represent the tangential stress, normal stress, and normal stress component along the crack direction; $\overset{i}{u}_s$ and $\overset{i}{u}_n$ represent the displacement of unit $i$ in the tangential and normal directions; $\overset{j,i}{A}_{ss}$, $\overset{j,i}{A}_{sn}$, $\overset{j,i}{A}_{ns}$, $\overset{j,i}{A}_{nn}$, $\overset{j,i}{A}_{ts}$, and $\overset{j,i}{A}_{tn}$ represent the stress influence coefficients; and $\overset{j,i}{B}_{ss}$, $\overset{j,i}{B}_{sn}$, $\overset{j,i}{B}_{ns}$, and $\overset{j,i}{B}_{nn}$ represent the displacement influence coefficient.

When a crack is equally divided into N crack units, the stress and displacement components formed at unit $i$ are produced by the joint action of the displacement discontinuities of the N crack units, specifically expressed as follows:

$$\begin{cases} \overset{i}{\sigma}_s = \sum\limits_{j=1}^{N} \overset{j,i}{A}_{ss}\overset{j}{D}_s + \sum\limits_{j=1}^{N} \overset{j,i}{A}_{sn}\overset{j}{D}_n \\ \overset{i}{\sigma}_n = \sum\limits_{j=1}^{N} \overset{j,i}{A}_{ns}\overset{j}{D}_s + \sum\limits_{j=1}^{N} \overset{j,i}{A}_{nn}\overset{j}{D}_n \\ \overset{i}{\sigma}_t = \sum\limits_{j=1}^{N} \overset{j,i}{A}_{ts}\overset{j}{D}_s + \sum\limits_{j=1}^{N} \overset{j,i}{A}_{tn}\overset{j}{D}_n \\ \overset{i}{u}_s = \sum\limits_{j=1}^{N} \overset{j,i}{B}_{ss}\overset{j}{D}_s + \sum\limits_{j=1}^{N} \overset{j,i}{B}_{sn}\overset{j}{D}_n \\ \overset{i}{u}_n = \sum\limits_{j=1}^{N} \overset{j,i}{B}_{ns}\overset{j}{D}_s + \sum\limits_{j=1}^{N} \overset{j,i}{B}_{nn}\overset{j}{D}_n \end{cases} \tag{7}$$

For four boundary unit components, we need to obtain two components at the same time to solve, giving 2N linear algebra equations based on N discretized units. By using Formula (7) to list 2N independent linear algebraic equations for the boundary conditions given on all boundary elements, all 2N displacement discontinuity unknowns on the boundary elements can be solved. During the simulation process, the software first uses Formula (7) to determine the displacement discontinuity of each boundary based on the input stress value. Then, based on the displacement discontinuities of each boundary, the displacement and stress values of any point in the plane are obtained by superimposing them. This will generate new surface force components at the boundary, and then continue to calculate the displacement discontinuity at the boundary, iterating repeatedly to simulate crack propagation.

*2.2. Rock Fracture Criteria*

The stress intensity factor is a key factor influencing the propagation trajectory of hydraulic fractures. Under external loading, stress concentrations are formed at the tips of fractures in rocks, and their fracture types are divided into three types: opening (Mode I), sliding (Mode II), and tearing (Mode III) [31]. The stress intensity factor can be used to characterize the stress and displacement fields at the crack tip position [32]. $K_I$, $K_{II}$, and $K_{III}$ are the stress intensity factors at the tips of the three types of cracks, where $K_I$ and $K_{II}$ can be expressed as follows:

$$\begin{cases} K_I = \lim\limits_{r\to 0}\sqrt{2\pi r}\sigma_n = \lim\limits_{r\to 0}\frac{\sqrt{2}Ga}{\sqrt{\pi}(1-v)}\left[\frac{1}{(2a-r)\sqrt{r}}\right]D_n \\ K_{II} = \lim\limits_{r\to 0}\sqrt{2\pi r}\sigma_s = \lim\limits_{r\to 0}\frac{\sqrt{2}Ga}{\sqrt{\pi}(1-v)}\left[\frac{1}{(2a-r)\sqrt{r}}\right]D_s \end{cases} \tag{8}$$

The maximum circumferential stress criterion [33] is used to judge the crack initiation and extension direction, where the stress expression is as follows:

$$\begin{cases} \sigma_r = \frac{1}{2\sqrt{2\pi r}}\left[K_I(3-\cos\theta\cos\frac{\theta}{2}) + K_{II}(3\cos\theta - 1)\sin\frac{\theta}{2}\right] \\ \sigma_\theta = \frac{1}{2\sqrt{2\pi r}}\cos\frac{\theta}{2}[K_I(1+\cos\theta) - 3K_{II}\sin\theta] \\ \tau_{r\theta} = \frac{1}{2\sqrt{2\pi r}}\cos\frac{\theta}{2}[K_I\sin\theta + K_{II}(3\cos\theta - 1)] \end{cases} \tag{9}$$

According to the maximum circumferential stress criterion, cracks will initiate along the direction where the circumferential stress, $\sigma_\theta$, is the largest, where the value of the maximum circumferential stress is as follows:

$$(\sigma_\theta)_{\max} = \frac{1}{2\sqrt{2\pi r}}\cos\frac{\theta}{2}[K_I(1+\cos\theta) - 3K_{II}\sin\theta] \tag{10}$$

When the circumferential stress in the direction of the crack initiation angle, $\theta$, reaches the maximum value, that is, the critical value, $\sigma_c$, the crack begins to extend forward. From this, it can be obtained that the conditions for judging crack propagation based on the maximum circumferential stress criterion are as follows:

$$(\sigma_\theta)_{\max} = (\sigma_\theta)_c \tag{11}$$

The accuracy of the numerical model established in this paper has been verified in simulating hydraulic fracture propagation and induced stress field distribution. The specific methods and procedures of verification can be found in the literature [29,30] and are therefore not described in this section.

*2.3. Fracture Propagation Model Establishment*

To explore the interaction and propagation mechanisms of horizontal-well cluster spacing under different fracturing sequences, we developed a two-dimensional numerical simulation model for hydraulic fracture propagation, depicted in Figure 3. The model is based on several fundamental assumptions: (1) the reservoir is treated as a homogeneous, infinitely large ideal linear elastic body; (2) hydraulic fracture deformation is modeled using two-dimensional plane strain conditions in the $x$ and $y$ directions; and (3) the model neglects fluid loss during fracturing and does not account for pressure gradients within the fractures. The proposed model cannot be used to analyze fracture propagation in highly permeable reservoirs or under ultralow-viscosity fracturing fluid conditions. Another drawback of the model is that it cannot take into account the heterogeneity of reservoir rock mechanical properties.

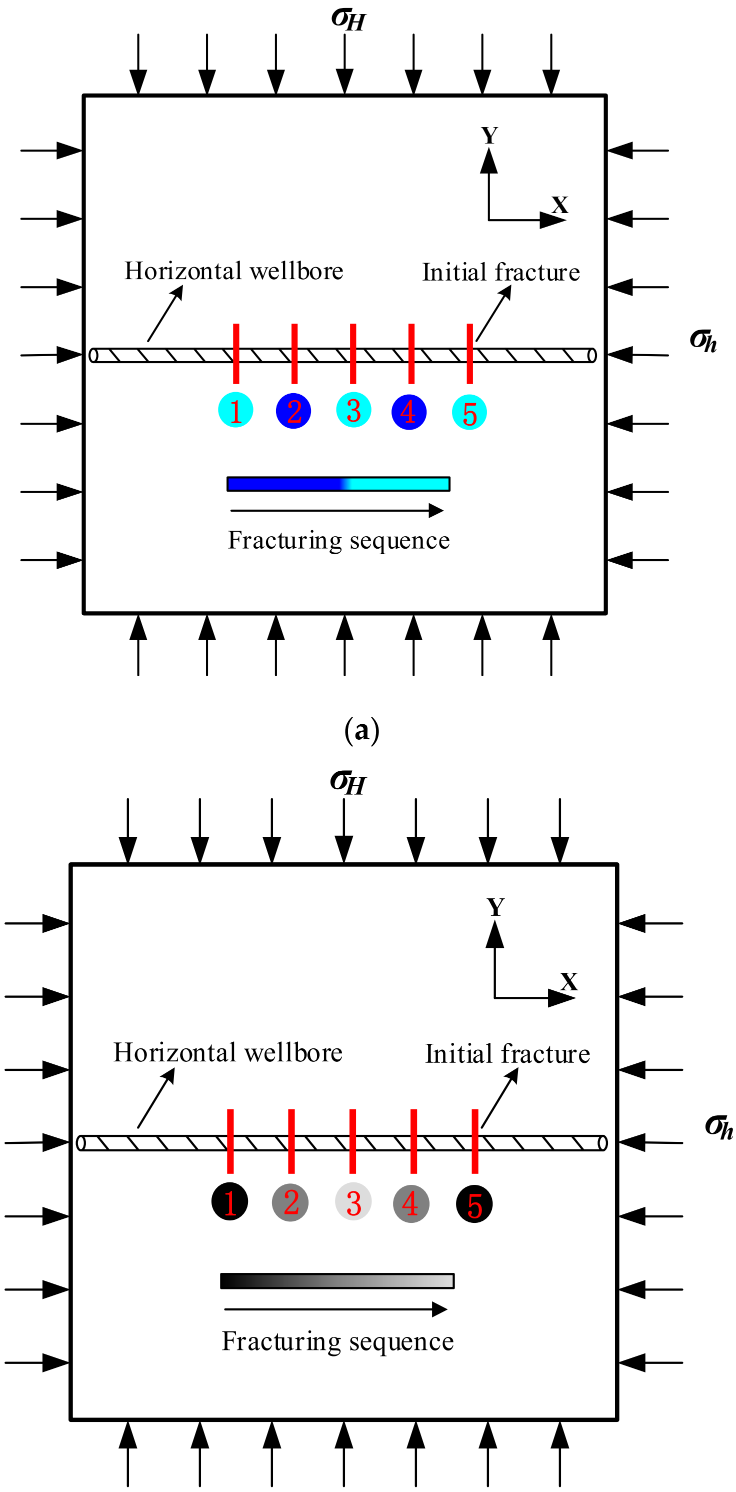


(**b**)

**Figure 3.** (**a**) Numerical simulation model of crack growth for alternating fracturing. (**b**) Numerical simulation model for crack growth for symmetrical fracturing.

As shown in Figure 3, a uniform and symmetrical application of maximum horizontal principal stress ($\sigma_H$) and minimum horizontal principal stress ($\sigma_h$) is imposed on the boundaries of the numerical model to simulate the effect of in situ stress. Within each individual fracturing segment of the horizontal wellbore, five short initial fractures are pre-set to simulate the interaction mechanisms of five competing clusters of fractures. By controlling the timing of fracturing fluid injection, we designed two different fracturing sequences: alternating fracturing (Figure 3a) and symmetrical fracturing (Figure 3b). Given the ease of implementation using temporary plugging fracturing technology and their suitability for controlling the simulation process and comparing induced stress fields, we ultimately selected these two standardized fracturing sequences for our research. Taking alternating fracturing as an example, we first injected fracturing fluid into initial fractures 2 and 4. Under constant pressure, fractures 2 and 4 begin to propagate. Once fractures 2 and 4 have expanded to a certain length, fracturing fluid injection is halted to maintain fracture internal pressure. Subsequently, fracturing fluid is injected into initial fractures 1, 3, and 5, and the propagation morphology of subsequent fractures under constant internal pressure is observed. The basic parameters of the numerical model are listed in Table 1. It is noted that compressive stress is represented as negative values, while tensile stress is represented as positive values in this study.

**Table 1.** Numerical model parameter table.

| Category | Numerical Value |
|---|---|
| Young's modulus/MPa | 20,400 |
| Poisson's ratio | 0.23 |
| Maximum horizontal principal stress $\sigma_H$/MPa | 32 |
| Minimum horizontal principal stress $\sigma_h$/MPa | 30 |
| Fracture toughness/ MPa·m$^{1/2}$ | 2.5 |
| Rock density/kg·m$^{-3}$ | 2480 |

## 3. Discussion of Simulation Results

### 3.1. Alternating Fracturing

(1) Influence of cluster spacing

Figure 4 illustrates the fracture propagation morphology of alternating fracturing under the same fracture internal pressure but different cluster spacing. After fractures 2 and 4 have propagated 50 m and terminated to maintain fracture internal pressure, fracturing fluid is injected into fractures 1, 3, and 5. The internal pressure within each cluster fracture remains consistent during the fracturing process. The induced normal stress field and shear stress field around the fractures are shown in Figures 5 and 6, respectively. As depicted in Figure 4, when the cluster spacing is only 15 m, fractures 1, 3, and 5 cannot initiate propagation after the previous fractures 2 and 4 have terminated propagation. Fractures 2 and 4 exhibit mutually repulsive propagation behavior. When the cluster spacing increases to 25 m, fractures 1 and 5 can initiate propagation after the previous fractures 2 and 4 have propagated, while fracture 3 still cannot initiate propagation. Fractures 2 and 4 propagate in a linear manner, with the weakening of the repulsive interaction. However, fractures 1 and 5 exhibit noticeable deviation after initiation (indicated by blue dashed lines in Figure 4b), propagate while repulsing each other, and the deviation gradually diminishes with increasing propagation length. When the cluster spacing further increases to 35 m, fracture 3 still cannot initiate propagation, but the repulsive interaction between fractures 1 and 5 weakens (indicated by blue dashed lines in Figure 4c). When the cluster spacing reaches 45 m, fracture 3 can initiate propagation, and the deviation of fractures 1 and 5 decreases after initiation (indicated by blue dashed lines in Figure 4d).

Figure 5 illustrates that, when the cluster spacing is 15 m, the pressure stress field around the previously fractured fractures 2 and 4 is strong, placing the subsequent fractures 1, 3, and 5 in a high-pressure stress zone, thereby preventing their initiation and propagation. As the cluster spacing increases, the pressure stress around the previously fractured fractures significantly decreases, enabling the initiation and propagation of subsequent fractures 1 and 5. The pressure stress distribution around the wellbore vicinity of the subsequent fractures 1 and 5 is asymmetric, with stronger pressure stress on the inner side than on the outer side, resulting in the deflection of subsequent fractures 1 and 5 after initiation. When the cluster spacing increases to above 35 m, the pressure stress acting on the region where subsequent fracture 3 is located has significantly reduced, initiating its propagation. Figure 6 shows that, when the cluster spacing is 15 m, the shear stress field on the outer side of the previously fractured fractures 2 and 4 is significantly stronger than on the inner side. Consequently, in situations with small cluster spacing, subsequent fractures cannot initiate, but natural fractures on the outer side may experience shear slip induced by the shear stress field. With an increase in cluster spacing, subsequent fractures can initiate and propagate, resulting in a substantial attenuation of the shear stress field around the previously fractured fractures that mainly concentrates on the outer side of the subsequent fractures. When the cluster spacing increases to 45 m, subsequent fracture 3 can initiate and propagate, enhancing the shear stress in the central region. Therefore, the comprehensive analysis of Figures 4–6 suggests that it is advisable to appropriately increase the cluster spacing during alternate fracturing to mitigate the inhibitory effect of previously fractured fractures on subsequent ones. A reasonable cluster spacing not only facilitates effective propagation of fractures within each segment but also diminishes the induced pressure stress field from previously fractured fractures, enhancing the shear stress around fractures within the cluster.

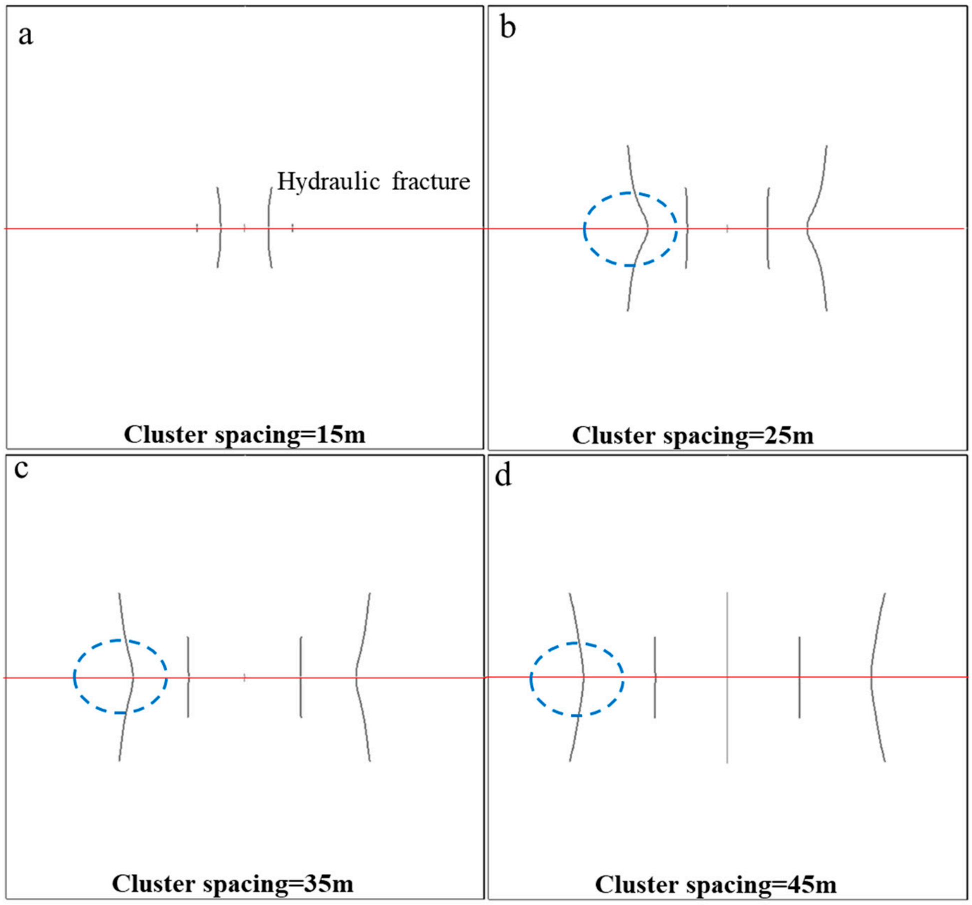


**Figure 4.** Alternate fracturing fracture propagation patterns under different cluster spacing (fracture internal pressure is 34 MPa).

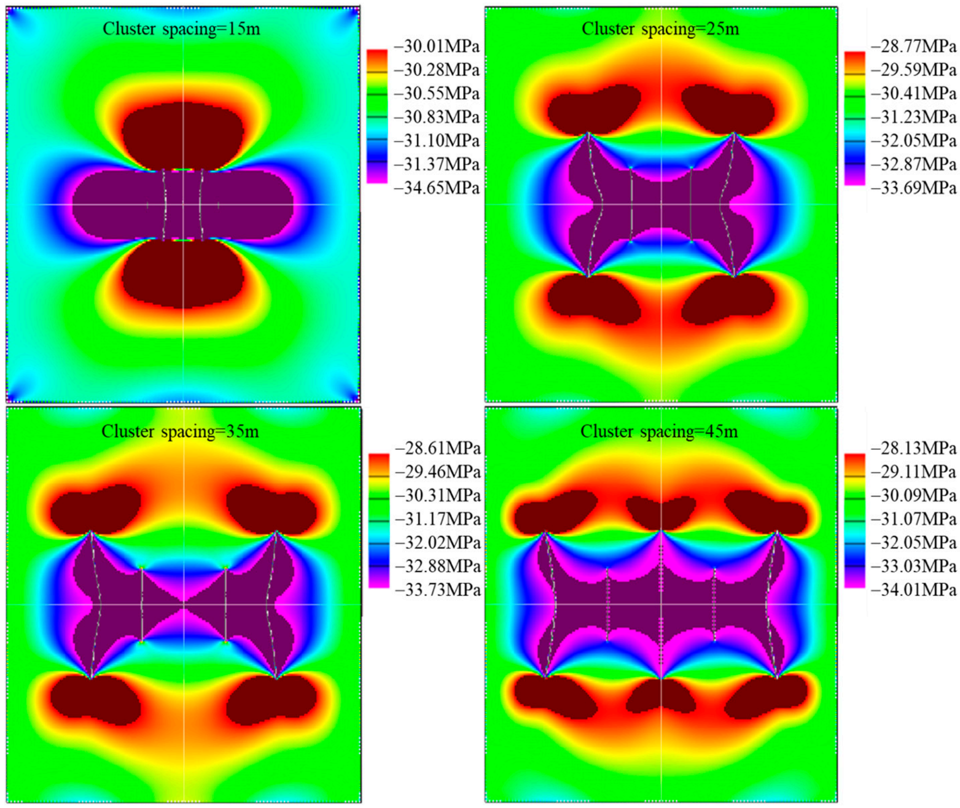


**Figure 5.** Normal stress field in X direction around fractures of alternating fracturing under different cluster spacing.

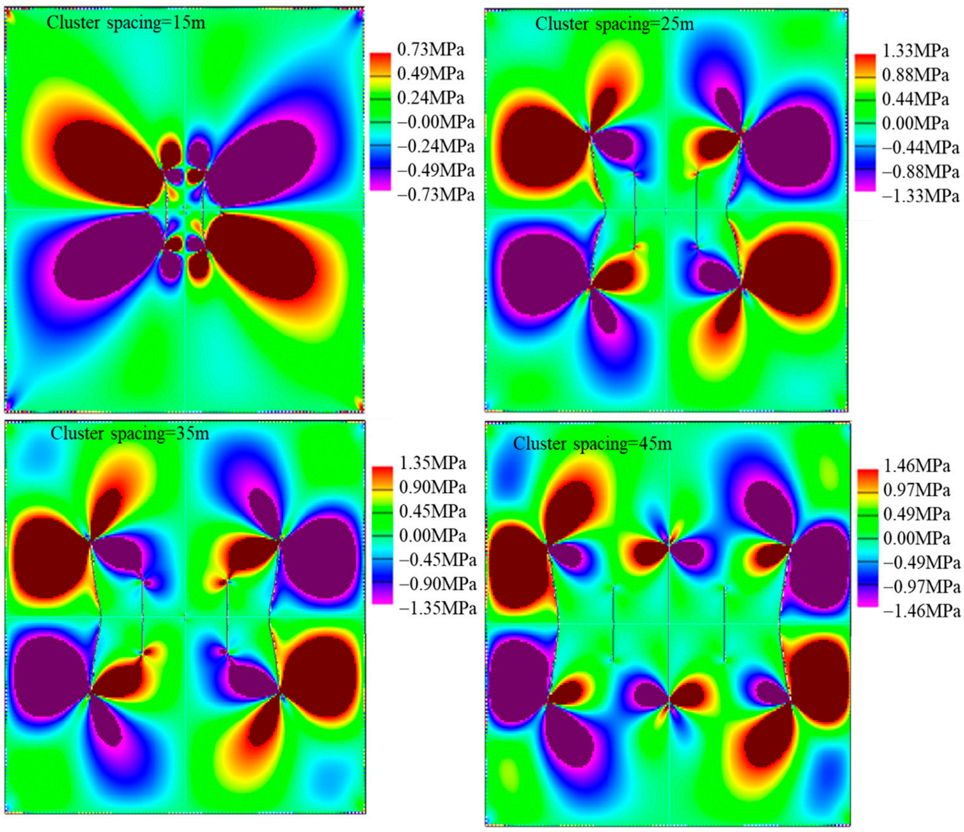


**Figure 6.** Shear stress field around fractures of alternating fracturing under different cluster spacing.

(2) Effect of fracture internal pressure

During hydraulic fracturing, while keeping reservoir rock properties constant, varying the fracturing fluid volume significantly influences the fracture internal pressure, consequently leading to different fracture propagation patterns. We analyzed the fracture propagation patterns during alternate fracturing under the same cluster spacing but different fracture internal pressure conditions. In the simulation process, after the initiation of previously fractured fractures, we used the fracture internal pressure of the previously fractured fractures as the initial value and gradually increased the fracture internal pressure of subsequent fractures until a change occurred. As shown in Figure 7a, after fractures 2 and 4 initiated and expanded at 31.0 MPa, subsequent fractures could not initiate and propagate at the same pressure. When the fracture internal pressure of the subsequent fractures increased to 31.7 MPa (Figure 7b), fractures 1 and 5 could initiate and propagate, while fracture 3 still could not initiate and propagate. When the fracture internal pressure of subsequent fractures further increased to 31.9 MPa (Figure 7c), fractures 1 and 5 initiated and propagated to a certain length before fracture 3 began to initiate and propagate, resulting in a shorter final propagation length for fracture 3. When the fracture internal pressure of the subsequent fractures increased to 32.0 MPa (Figure 7d), fractures 1, 3, and 5 initiated and propagated simultaneously, resulting in a similar final propagation length for subsequent fractures. In this paper, the term "deflection effect" describes the phenomenon where a fracture reorients under induced stress, causing its propagation trajectory to deviate from the direction of maximum horizontal principal stress. Additionally, comparing Figure 7b with Figure 4b reveals that increasing the fracture internal pressure of subsequent fractures compared to previously fractured fractures effectively mitigates the deflection effect of subsequent fractures. Overall, as depicted in Figure 7, after the completion of previously fractured fractures, increasing the fluid volume to enhance the fracture internal pressure of subsequent fractures facilitates overcoming the inhibitory effect of previously fractured fractures on subsequent ones.

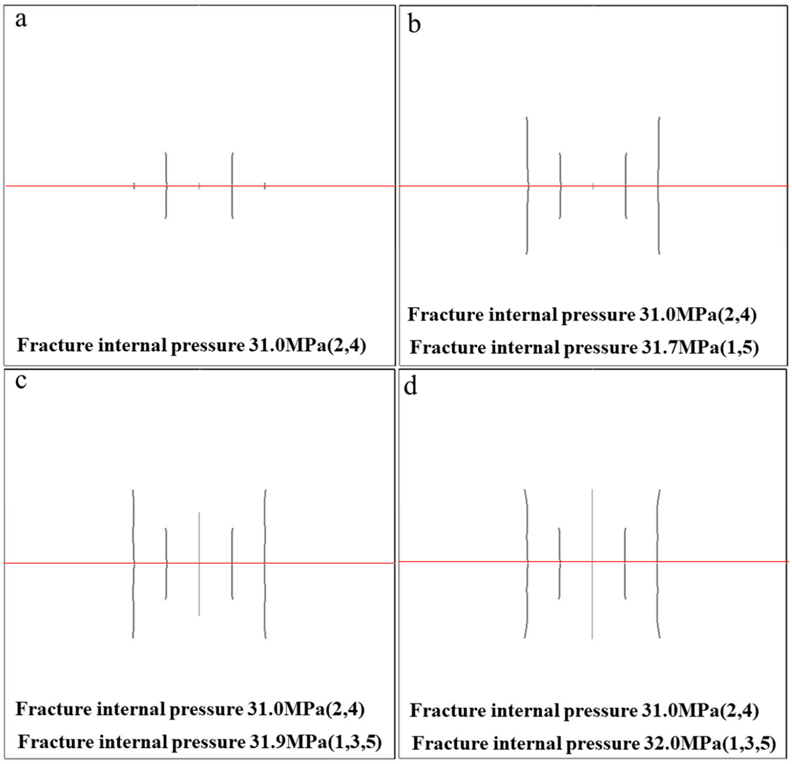


**Figure 7.** Fracture growth patterns of alternating fracturing under different intra-fracture pressures (cluster spacing, 25 m).

Figure 8 depicts the induced stress field distribution around the fractures corresponding to Figure 7. It can be observed from Figure 8 that, under low fracture internal pressure conditions, the strong pressure stress zone formed by previously fractured fractures is extensive, thereby inhibiting the initiation and propagation of subsequent fractures. As the fracture internal pressure of subsequent fractures increases, these fractures can initiate and propagate. The strong pressure stress zone within the previously fractured fractures significantly weakens, forming a rectangular region of weak pressure stress. In this region, the pressure stress field exhibits an X-shaped symmetrical distribution, surrounded by the strong pressure stress zone formed by subsequent fractures. With an increase in internal pressure, the propagation of subsequent fractures 1 and 5 results in a slight reduction in the range of induced shear stress field on the outer side of the fractures but enhances the heterogeneity of the shear stress field distribution on the inner side of the fractures. Overall, increasing the fracture internal pressure of subsequent fractures helps weaken the pressure stress effect caused by previously fractured fractures and enhances the shear action on the inner side of the fractures.

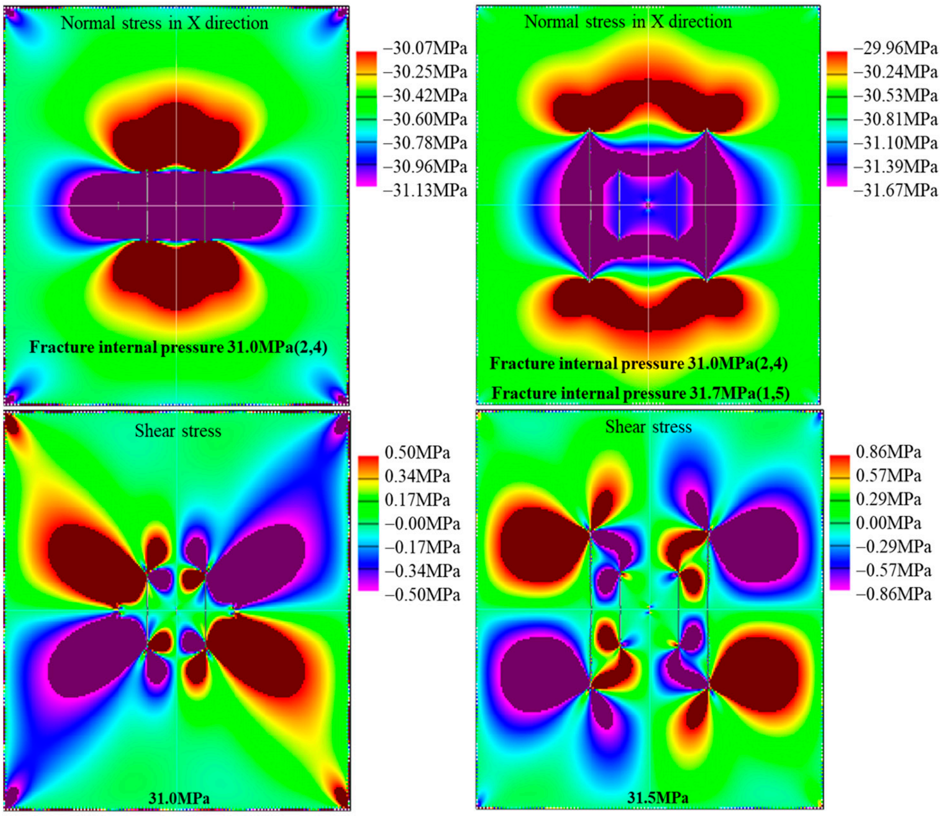


**Figure 8.** Induced stress field around fractures of alternating fracturing under different intra-fracture pressures (cluster spacing 25 m).

(3) Influence of the length of previously fractured fractures

The extension length of previously fractured fractures affects the propagation pattern of subsequent fractures. We analyzed the propagation patterns and induced stress field distribution of alternating fracturing fractures under different extension lengths of previously fractured fractures, as depicted in Figure 9. In this section, the extension length of previously fractured fracture 2 is defined as L. As illustrated in Figure 9, when the extension length of previously fractured fractures is relatively short, subsequent fractures can initiate and propagate under the same internal pressure. The deflection amplitude of subsequent fractures 1 and 5 is small. However, when the extension length of previously fractured fractures increases to 60 m, only subsequent fractures 1 and 5 can initiate and propagate, while subsequent fracture 3 cannot initiate. Moreover, under the same time step, the lengths of subsequent fractures 1 and 5 noticeably decrease, and the deflection amplitude increases after initiation. When the extension length of previously fractured fractures further increases to 70 m, the subsequent fractures 1, 3, and 5 cannot initiate and propagate. From the distribution of induced stress fields, it can be observed that, the shorter the length of previously fractured fractures, the weaker the induced pressure stress acting around the horizontal wellbore, which is more favorable for the initiation and propagation of subsequent fractures resulting from fracturing. As the extension length of previously fractured fractures increases, the enhanced pressure stress around the horizontal wellbore suppresses the initiation of subsequent fractures resulting from fracturing. In summary, during alternating fracturing, it is essential to design reasonable lengths for previously fractured fractures; otherwise, there is a risk of significantly inhibiting the initiation and propagation of subsequent fracturing fractures.

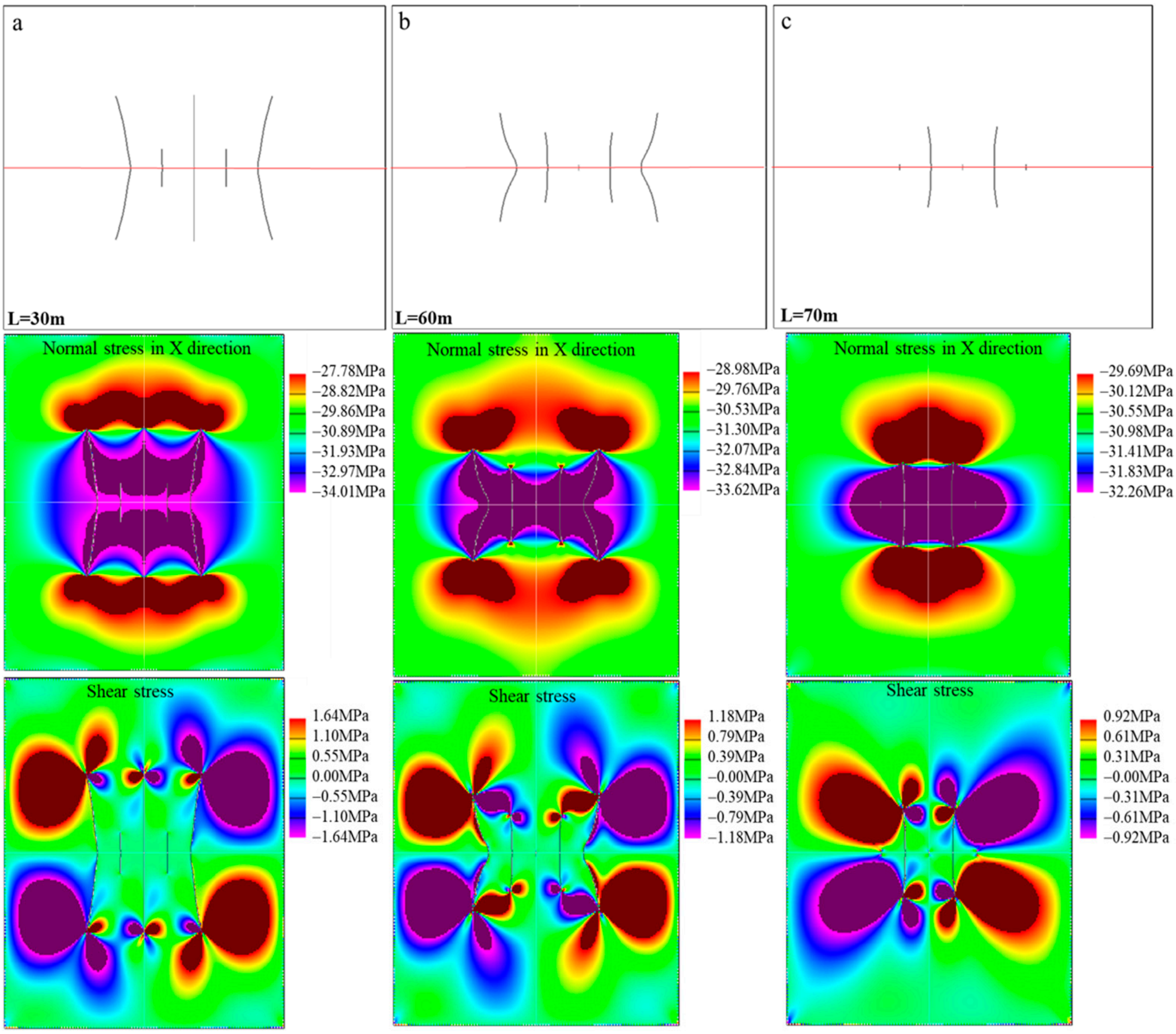


**Figure 9.** Fracture propagation morphology and corresponding induced stress field of alternating fracturing under different fracture lengths produced by previous fracturing (intra-fracture pressure, 34 MPa; cluster spacing, 25 m).

Figure 10 illustrates the critical extension length of previously fractured fractures required for subsequent fracturing fractures to initiate and propagate under different cluster spacing. Taking a cluster spacing of 15 m as an example, if the length of previously fractured fractures exceeds the value indicated by the red circle, subsequent fracture 3 cannot initiate and propagate. Similarly, if the length of previously fractured fractures exceeds the value indicated by the black square, subsequent fractures 1 and 5 cannot initiate and propagate. Therefore, to ensure the initiation and propagation of subsequent fracturing fractures, it is necessary to either reduce the length of previously fractured fractures at each point or increase the cluster spacing. Additionally, from Figure 10, it can be observed that as the cluster spacing increases, the critical extension length of previously fractured fractures for subsequent fractures 1 and 5 to initiate and propagate significantly increases. This indicates that, with larger cluster spacing, the difficulty of subsequent fractures 1 and 5 to initiate and propagate decreases substantially. However, as the cluster spacing increases, the increase in the critical extension length of previously fractured fractures for subsequent fracture 3 is relatively small. This suggests that the difficulty for subsequent fracture 3 to initiate decreases with increasing cluster spacing but remains higher than that for subsequent fractures 1 and 5. Figure 10 establishes a standard for selecting the critical extension length of previously fractured fractures.

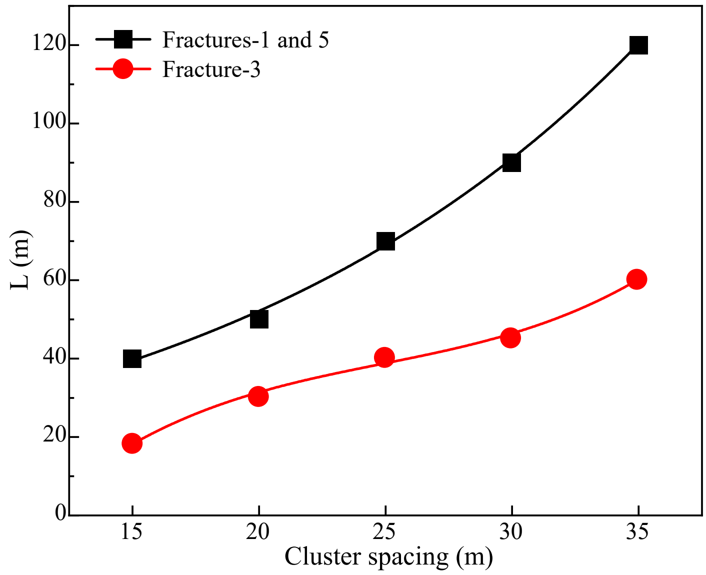


**Figure 10.** The critical length of previously fractured fractures at which subsequent fractures can initiate and expand under different cluster spacing (intra-fracture pressure is 34 MPa).

Critical fracture internal pressure is defined as the minimum fluid pressure necessary for a hydraulic fracture to initiate propagation from a static condition. Investigating critical fracture internal pressure is beneficial for establishing the appropriate range of injection pressures during fracturing operations. Figure 11 illustrates the critical fracture internal pressure required for subsequent fracturing fractures to initiate and propagate under different cluster spacing. Under the same cluster spacing, subsequent fracturing fractures can initiate and propagate when the fracture internal pressure is above the curve; otherwise, they cannot initiate and propagate. From Figure 11, it can be observed that when the cluster spacing is less than 15 m, subsequent fractures 1, 3, and 5 require the same fracture internal pressure of 31.8 MPa for initiation. However, as the cluster spacing increases, the required fracture internal pressure for subsequent fracture 3 to initiate increases by 0.1 MPa, while the required fracture internal pressure for subsequent fractures 1 and 5 linearly decreases. Based on the illustration in Figure 11, if the design of previously fractured fracture length cannot be altered, increasing the fracture internal pressure or decreasing the cluster spacing is necessary to ensure the normal initiation of subsequent fracturing fractures. Figure 12 depicts the critical fracture internal pressure required for subsequent fracturing fractures to initiate and propagate under different lengths of previously fractured fractures. As shown in Figure 12, with an increase in the length of previously fractured fractures, the required fracture internal pressure for subsequent fracturing fractures to initiate and propagate increases in a stepwise manner. When the length of previously fractured fractures increases to 80 m, the required fracture internal pressure for subsequent fracturing fractures to initiate and propagate essentially remains unchanged. To design longer fracture lengths as much as possible, it is necessary to increase the fracture internal pressure of subsequent fracturing fractures based on the illustration in Figure 12 to ensure their initiation and propagation.

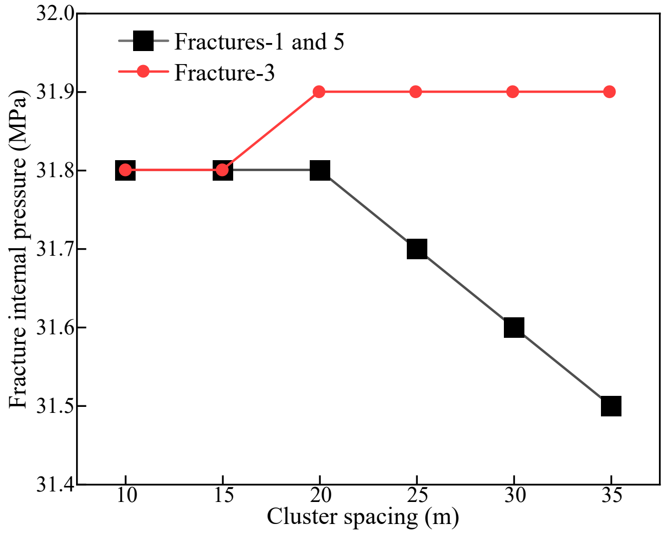


**Figure 11.** Critical intra-fracture pressure at which subsequent fracturing fractures can initiate and propagate under different cluster spacing (previously fracturing fractures 2 and 4 intra-fracture pressure = 31 MPa, previously fracturing fracture 2 length L = 50 m).

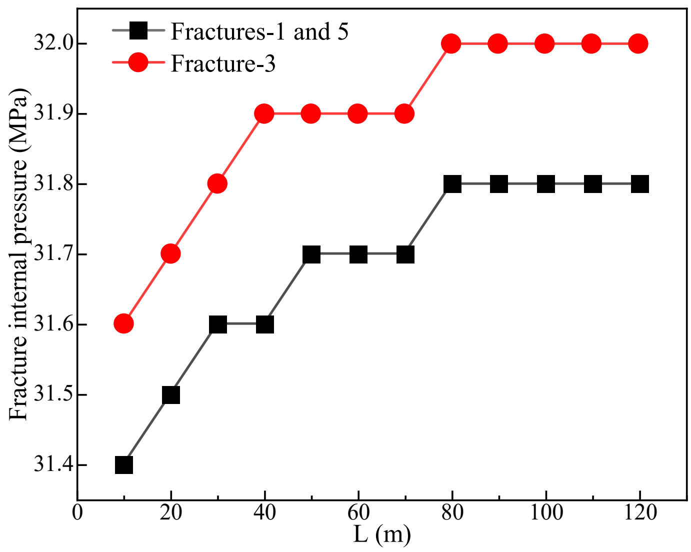


**Figure 12.** The critical intra-fracture pressure at which subsequent fracturing fractures can initiate and propagate under different previously fractured fracture lengths (previously fractured fractures 2 and 4 intra-fracture pressure = 31 MPa; cluster spacing = 25 m).

### *3.2. Symmetric Fracturing*

We investigated and analyzed the fracture propagation process of symmetric fracturing, as illustrated in Figure 13. To ensure the initiation and propagation of fractures in all five clusters, we set the fracture internal pressure of the previously fractured fractures 1 and 5 to 35 MPa; fractures 2 and 4, which were fractured subsequently, to 36 MPa; and the fracture internal pressure of the last one, fractured fracture 3, to 37 MPa. The cluster spacing was 10 m, and the designed fracture propagation length was 60 m. The fracture internal pressure was maintained after the initiation and propagation of the previously fractured fractures, followed by subsequent fracturing. As shown in Figure 13, after the initiation of the previously fractured fractures 1 and 5, the fracture propagation exhibited a symmetrical distribution, with minimal overall deviation of fractures (Figure 13b). Upon the initiation of fractures 2 and 4, which were fractured subsequently, initially, they propagated primarily in a direction perpendicular to the minimum horizontal principal stress; then, after propagating a certain length, they deviated to some extent and repelled each other during propagation (Figure 13c). Fractures 2 and 4, which were fractured subsequently, were gradually attracted and captured by the previously fractured fractures 1 and 5. After the initiation of the last fractured fracture, fractured fracture 3, it consistently propagated in a direction perpendicular to the minimum horizontal principal stress (Figure 13d). A comparison with Section 3.1 reveals that in symmetric fracturing, the morphology of fracture propagation is somewhat more complex. The variation in the deviation angles of fractures 1, 2, and 3 with fracture length is shown in Figure 14. We define the deviation angle of a fracture at a certain point as the angle between the tangent direction of the fracture and the direction of the maximum horizontal principal stress (clockwise as positive, counterclockwise as negative). As depicted in Figure 14, after the initiation of the previously fractured fracture 1, the deviation angle is minimal, and then, as the fracture length increases, the deviation angle slowly increases, with the overall deviation angle not exceeding 5°. After the initiation of the subsequently fractured fracture 2, it initially deviates clockwise by 10°. Subsequently, fracture 2 reorients and deviates counterclockwise significantly, with a maximum deviation angle exceeding 30°. Finally, as subsequent fractured fracture 2 approaches the previously fractured fracture 1, the deviation angle gradually decreases again, and subsequently fractured fracture 2 is gradually captured by the previously fractured fracture.

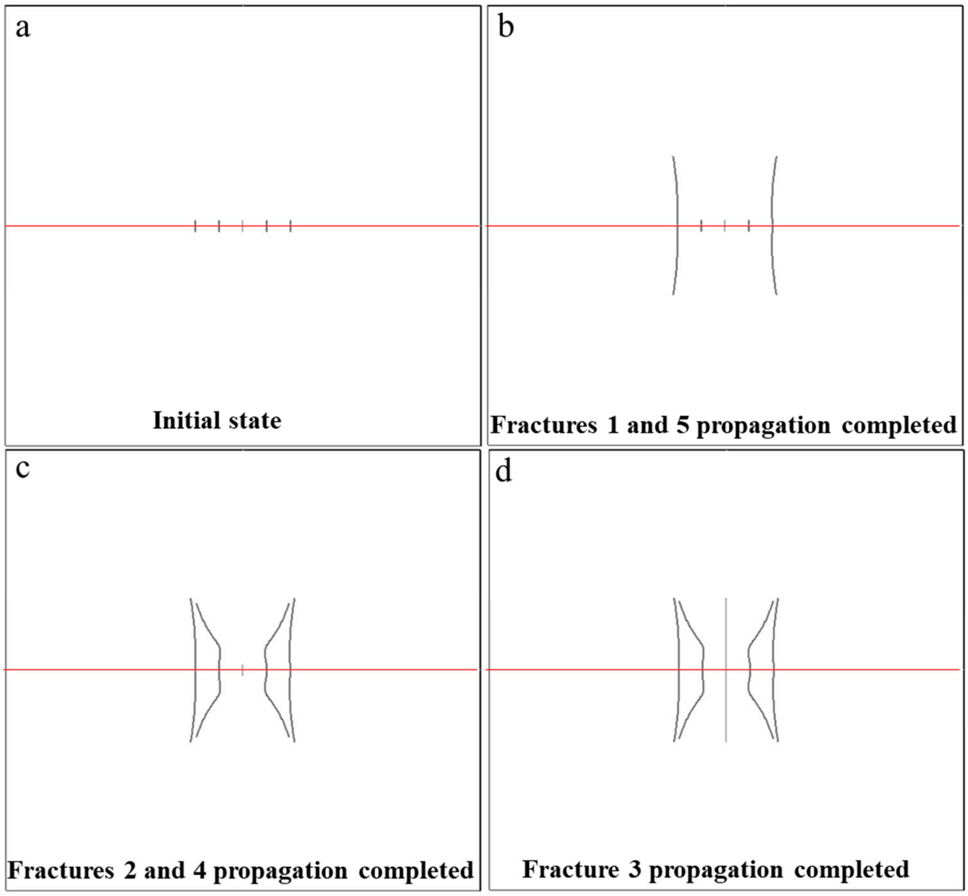


**Figure 13.** Symmetric fracturing crack growth process.

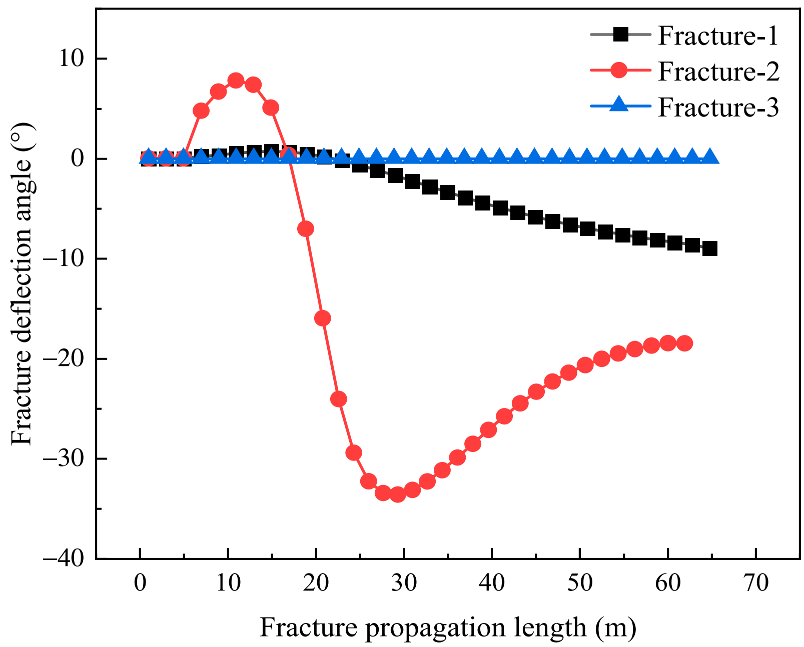


**Figure 14.** Crack deflection angle changes curve with crack length.

Figure 15 illustrates the variation in the induced stress field during the process of symmetric fracturing. From Figure 15, it can be observed that, after the completion of propagation of the previously fractured fractures 1 and 5, the tensile effect at the tips of the fractures is relatively weak, and there is a wide range of compressive stress around the horizontal wellbore. The shear stress field is mainly concentrated on the outer side of the fractures, with weak shear action on the inner side of the fractures. Upon completion of the propagation of the subsequently fractured fractures 2 and 4, the tensile effect at the tips of the fractures and the shear action on the inner side of the fractures are enhanced, while the compressive stress around the horizontal wellbore is weakened. Due to the weaker compressive stress on the inner side of the fractures compared to the outer side, subsequently fractured fractures 2 and 4 tend to deviate towards the direction of the previously fractured fractures 1 and 5. After the completion of the propagation of the last fractured fracture, fractured fracture 3, the compressive stress around the horizontal wellbore and the tensile effect at the tips of the fractures are enhanced, and the non-uniformity of the shear stress on the inner side of the fractures is increased. A comparison with the content of Section 3.1 reveals that symmetric fracturing tends to enhance the shear action on the inner side of the fractures, thereby facilitating shear failure along natural fractures.

Figure 16 depicts the morphology of symmetric fracturing and the distribution of induced stress fields under different cluster spacing. It is evident from Figure 16 that the cluster spacing significantly affects the morphology of symmetric fracturing. When the cluster spacing is small (Figure 16a,b), subsequently fractured fractures 2 and 4 are attracted and gradually captured by the previously fractured fractures 1 and 5. When the cluster spacing is large, subsequently fractured fractures 2 and 4 exhibit a wave-like propagation pattern. The distribution of induced stress fields reveals that changing the cluster spacing affects the shape of the deep red tensile stress zone at the tips of the fractures. A smaller cluster spacing results in a more flattened compressive stress zone around the horizontal wellbore. Increasing the cluster spacing significantly enhances the non-uniform distribution of shear stress on the inner side of the fractures. Taking fracture 2 as an example, we analyzed the effect of cluster spacing on the deviation angle of the fractures, as shown in Figure 17. It can be observed from Figure 17 that a smaller cluster spacing leads to a faster deviation rate after the initiation of subsequently fractured fracture 2. Increasing the cluster spacing slows down the magnitude of deviation of subsequently fractured fracture 2 near the wellbore. With the increasing fracture length, subsequently fractured fracture 2 is less likely to be captured under larger cluster spacing. In conclusion, based on the above analysis, it is advisable to select an appropriate cluster spacing to prevent subsequently fractured fractures from being captured by previously fractured fractures when employing symmetric fracturing.

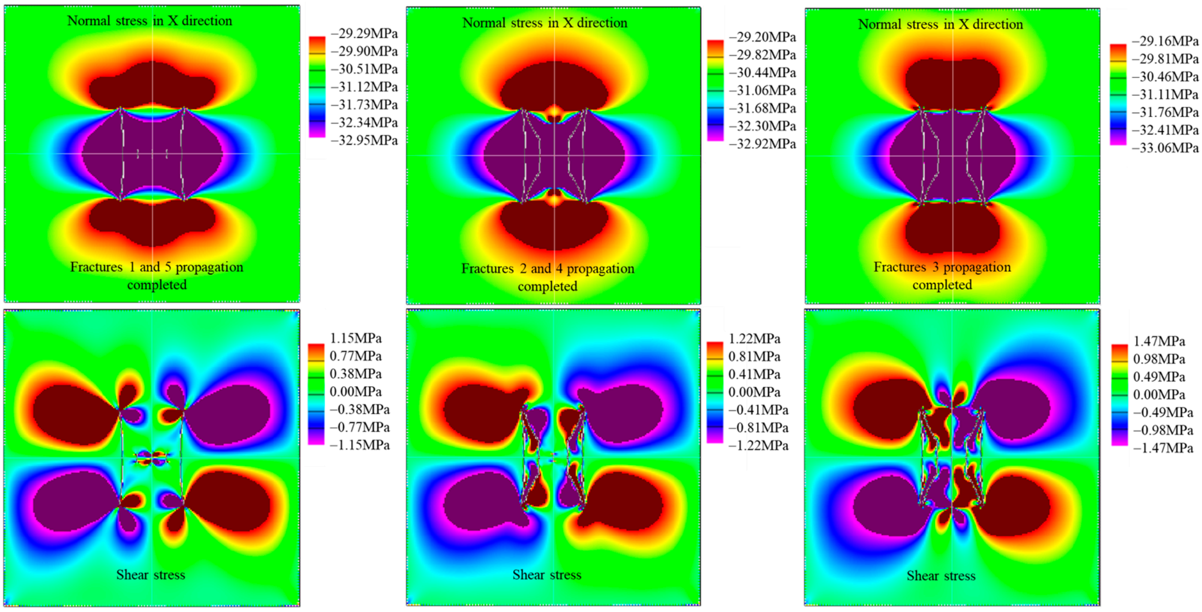


**Figure 15.** Changes in the induced stress field during the crack propagation process of symmetrical fracturing.

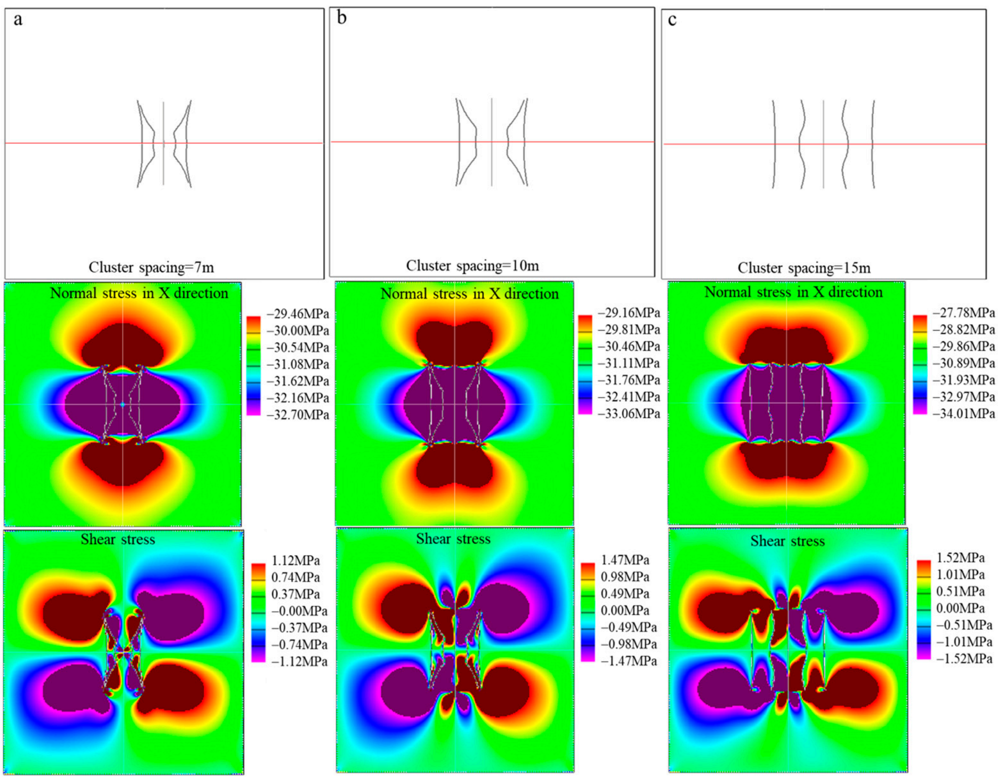


**Figure 16.** Fracture propagation morphology and induced stress field distribution of symmetrical fracturing under different cluster spacing.

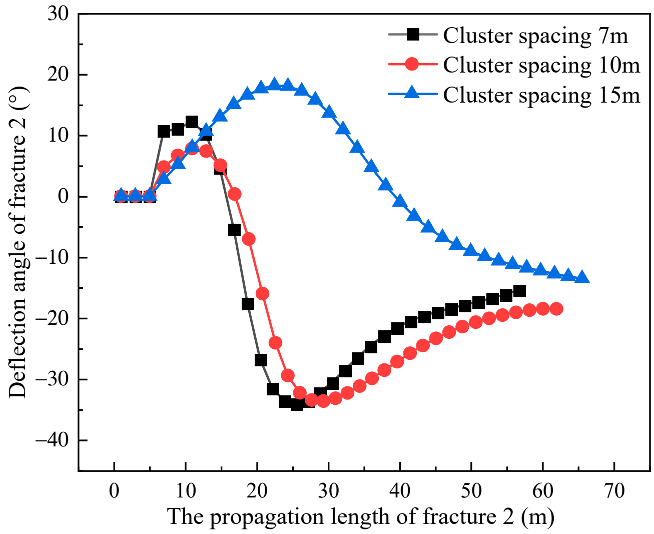


**Figure 17.** Variation curve of fracture 2 deflection angle with length for symmetrical fracturing under different cluster spacing.

We analyzed the critical fracture internal pressure required for the initiation and propagation of subsequently fractured fractures 2 and 4, as well as fracture 3, under different cluster spacing, as shown in Figure 18. It can be observed from Figure 18 that, with increasing cluster spacing, the critical fracture internal pressure required for the initiation and propagation of subsequently fractured fractures 2 and 4 decreases slowly, while the critical fracture internal pressure required for the initiation and propagation of the last fractured fracture, fractured fracture 3, increases linearly. This indicates that increasing the cluster spacing can reduce the initiation difficulty of subsequently fractured fractures 2 and 4, but it increases the initiation difficulty of intermediate fracture 3.

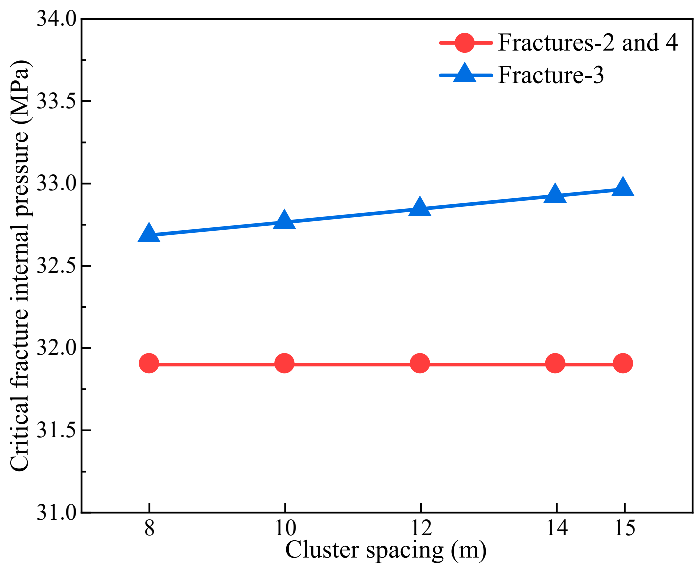


**Figure 18.** Critical intra-fracture pressure at which subsequent fracturing fractures can initiate and propagate under different cluster spacing (intra-fracture pressure of previously fractured fractures 1 and 5 = 31 MPa).

Figure 19 illustrates the morphology of symmetric fracturing and the corresponding distribution of induced stress fields under different critical fracture internal pressures. Fractures 1 and 5, which were previously fractured, initiate and propagate under two different internal pressure conditions, 31.0 MPa and 34.0 MPa, respectively. Subsequently, fractured fractures (2, 4, 3) initiate and propagate based on their respective critical fracture internal pressures. It can be observed from Figure 19 that, as the internal pressure within fractures 1 and 5 decreases, the critical pressure required for subsequent fractures (2, 4, 3) to initiate decreases accordingly. When the internal pressure within previously fractured fractures is relatively low (Figure 19a), subsequently fractured fractures 2 and 4 are attracted by the previously fractured fractures 1 and 5, resulting in the opposing propagation of fractures. Conversely, when the internal pressure within previously fractured fractures is relatively high (Figure 19b), subsequently fractured fractures 2 and 4 are attracted to each other, leading to the co-propagation of fractures. The distribution of induced stress fields reveals that, when the internal pressure within previously fractured fractures is relatively low, the compressive stress zone around the horizontal wellbore appears more uniform and rounded. The distribution area of shear stress on the inner side of the fractures is larger and more uniform. Increasing the internal pressure within previously fractured fractures results in a flatter and more uneven distribution of compressive stress zones around the horizontal wellbore, and the area of shear stress on the inner side of the fractures becomes smaller. In conclusion, based on the above analysis, for symmetric fracturing, it is advisable to use smaller injection volumes to reduce internal pressure and weaken the mutual attraction between fractures.

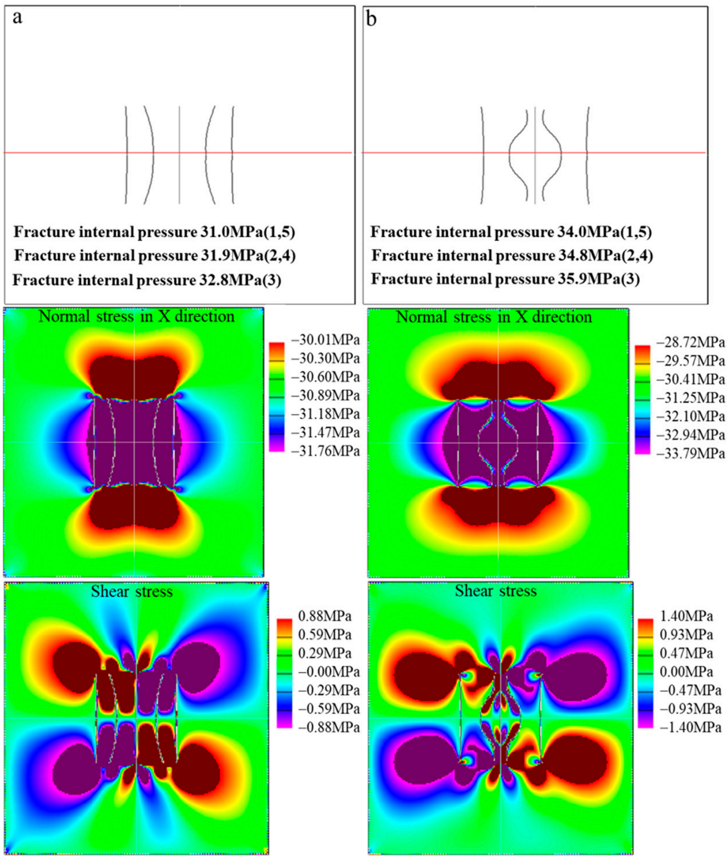


**Figure 19.** Fracture propagation morphology and corresponding induced stress field distribution of symmetrical fracturing under different critical intra-fracture pressures (cluster spacing 15 m).

## 4. Conclusions

Based on the theory of rock fracture mechanics and utilizing the boundary element method with displacement discontinuity, this study established a numerical simulation model for the interaction and propagation of fractures between clusters in horizontal wells. Based on this model, the competitive propagation morphology of fractures and the mechanism of induced stress fields under alternating fracturing and symmetric fracturing were analyzed. The main conclusions of this study are as follows:

(1) When employing alternating fracturing, it is advisable to increase the cluster spacing appropriately to mitigate the inhibitory effect of previously fractured fractures on subsequently fractured fractures. A reasonable cluster spacing not only facilitates the effective propagation of fractures within each segment but also reduces the compressive stress induced by previously fractured fractures, thus enhancing the surrounding shear stress.
(2) For alternating fracturing, increasing the internal pressure within subsequently fractured fractures can effectively mitigate the deviation effect, thereby helping subsequently fractured fractures overcome the inhibitory effect of induced compressive stress from previously fractured fractures. As the length of previously fractured fractures increases, the enhanced compressive stress around the horizontal wellbore inhibits the initiation of subsequently fractured fractures.
(3) Compared to alternating fracturing, symmetric fracturing results in more complex fracture propagation morphology. Under the same cluster spacing, symmetric fracturing enhances the shear action on the inner side of fractures, facilitating shear failure along natural fractures.
(4) When employing symmetric fracturing, it is advisable to increase the cluster spacing appropriately to prevent subsequently fractured fractures from being captured by previously fractured fractures. Using smaller injection volumes during fracturing can effectively reduce internal pressure and weaken the mutual attraction between fractures.

**Author Contributions:** Conceptualization, X.C.; Methodology, X.C.; Software, W.Z.; Validation, W.Z.; Formal analysis, T.H.; Investigation, T.H.; Resources, X.D.; Data curation, X.D.; Writing—original draft, H.W.; Writing—review & editing, H.W.; Visualization, X.L.; Supervision, X.L. All authors have read and agreed to the published version of the manuscript.

**Funding:** This work was supported by the National Natural Science Foundation of China, grant numbers 51934005, U23B2089, and 52374038; and the Shaanxi Provincial Natural Science Basic Research Program Project, grant numbers 2024JC-YBQN-0554 and 2023-JC-QN-0427.

**Data Availability Statement:** The data used to support the findings of this study are available from the first author upon request, at wang_hai_yang@126.com.

**Conflicts of Interest:** Authors Xiaojun Cai, Weixuan Zhao, Tianbao Hu, Xinwei Du were employed by the companies Changqing Oilfield Company, China National Petroleum Corporation. The remaining authors declare that the research was conducted in the absence of any commercial or financial relationships that could be construed as a potential conflict of interest.

## References

1. Casero, A. 20 Years of Horizontal Multistage Completions: A Summary of Industry Evolution in Unconventional and Conventional Plays. In Proceedings of the Abu Dhabi International Petroleum Exhibition and Conference, Abu Dhabi, United Arab Emirates, 15–18 November 2021; SPE: Bellingham, WA, USA, 2021.
2. Heider, Y. A review on phase-field modeling of hydraulic fracturing. *Eng. Fract. Mech.* **2021**, *253*, 107881. [CrossRef]
3. Zhang, Q.; Zhang, X.-P.; Sun, W. A review of laboratory studies and theoretical analysis for the interaction mode between induced hydraulic fractures and pre-existing fractures. *J. Nat. Gas Sci. Eng.* **2021**, *86*, 103719. [CrossRef]
4. Lei, Q.; Xu, Y.; Cai, B.; Guan, B.; Wang, X.; Bi, G.; Li, H.; Li, S.; Ding, B.; Fu, H.; et al. Progress and prospects of horizontal well fracturing technology for shale oil and gas reservoirs. *Pet. Explor. Dev.* **2022**, *49*, 191–199. [CrossRef]
5. Ismail, A.; Azadbakht, S. A comprehensive review of numerical simulation methods for hydraulic fracturing. *Int. J. Numer. Anal. Methods Géoméch.* **2024**, *48*, 1433–1459. [CrossRef]
6. Yin, P.F.; Yang, S.Q.; Ranjith, P.G. Anisotropic Mechanical Behaviors of Shale Rock and Their Relation to Hydraulic Fracturing in a Shale Reservoir: A Review. *Energies* **2024**, *17*, 1761. [CrossRef]
7. Uribe-Patino, J.A.; Casero, A.; Dall'Acqua, D.; Davis, E.; King, G.E.; Singh, H.; Rylance, M.; Chalaturnyk, R.; Zambrano-Narvaez, G. A Comprehensive Review of Casing Deformation During Multi-Stage Hydraulic Fracturing in Unconventional Plays: Characterization, Diagnosis, Controlling Factors, Mitigation and Recovery Strategies. In Proceedings of the SPE Hydraulic Fracturing Technology Conference and Exhibition, The Woodlands, TX, USA, 6–8 February 2024; SPE: Bellingham, WA, USA, 2024.
8. Carson, S.A. Independent and major equity market and commodity return sources around the time of hydraulic fracking and horizontal drilling revolution: A differences-in-decompositions approach. *Econ. Innov. New Technol.* **2024**, *33*, 26–44. [CrossRef]

9. Mogck, D.; Doucette, J. Performance Redefined: A Business-Centric Approach to Assessing Hydraulic Fracturing Execution. In Proceedings of the Hydraulic Fracturing Technology Conference and Exhibition, The Woodlands, TX, USA, 6–8 February 2024; SPE: Bellingham, WA, USA, 2024; p. D021S006R005.
10. Wang, H.; Yang, S.; Zhou, D.; Wang, Q. Influence of non-intersecting cemented natural fractures on hydraulic fracture propagation behavior. *J. Struct. Geol.* **2024**, *181*, 105111. [CrossRef]
11. Wu, J.; Wu, M.; Guo, Y.; Huang, H.; Zhang, Z.; Zhong, G.; Gui, J.; Lu, J. Study on multi-cluster fracturing simulation of deep reservoir based on cohesive element modeling. *Front. Energy Res.* **2024**, *11*, 1339895. [CrossRef]
12. Wang, Y.J.; Wang, B.; Su, H.; Chang, T.; Dong, R.C.; Li, L.Z.; Tang, W.Y.; Jiang, T.X.; Zhou, F.J. Mechanisms of fracture propagation from multi-cluster using a phase field based HMD coupling model in fractured reservoir. *Pet. Sci.* **2024**. [CrossRef]
13. Chang, X.; Wang, X.; Yang, C.; Guo, Y.; Wei, K.; Hu, G.; Jiang, C.; Li, Q.; Dou, R. Simulation and optimization of fracture pattern in temporary plugging fracturing of horizontal shale gas wells. *Fuel* **2024**, *359*, 130378. [CrossRef]
14. Li, J.; Zhu, Z.; Hua, W.; Wu, D.; Zhang, N.; Dong, S.; Guo, T. Numerical Simulation of Fracture Propagation during Temporary Plugging Staged Fracturing in Tight-Oil Horizontal Wells. *ACS Omega* **2024**, *9*, 18542–18555. [CrossRef] [PubMed]
15. Xiong, S.; Liu, S.; Weng, D.; Shen, R.; Yu, J.; Yan, X.; He, Y.; Chu, S. A Fractional Step Method to Solve Productivity Model of Horizontal Wells Based on Heterogeneous Structure of Fracture Network. *Energies* **2022**, *15*, 3907. [CrossRef]
16. Liu, N.; Zhang, Z.; Zou, Y.; Ma, X.; Zhang, Y. Propagation law of hydraulic fractures during multi-staged horizontal well fracturing in a tight reservoir. *Pet. Explor. Dev.* **2018**, *45*, 1129–1138. [CrossRef]
17. Wang, H.; Zhou, D. Mechanistic study on the effect of seepage force on hydraulic fracture initiation. *Fatigue Fract. Eng. Mater. Struct.* **2024**, *47*, 1602–1619. [CrossRef]
18. Zhang, D.; Dai, Y.; Ma, X.; Zhang, L.; Zhong, B.; Wu, J.; Tao, Z. An analysis for the influences of fracture network system on multi-stage fractured horizontal well productivity in shale gas reservoirs. *Energies* **2018**, *11*, 414. [CrossRef]
19. Chen, Z.; Liao, X.; Zhao, X.; Dou, X.; Zhu, L. Performance of horizontal wells with fracture networks in shale gas formation. *J. Pet. Sci. Eng.* **2015**, *133*, 646–664. [CrossRef]
20. Gehne, S.; Benson, P.M.; Koor, N.; Dobson, K.J.; Enfield, M.; Barber, A. Seismo-mechanical response of anisotropic rocks under hydraulic fracture conditions: New experimental insights. *J. Geophys. Res. Solid Earth* **2019**, *124*, 9562–9579. [CrossRef]
21. Cao, W.; Yildirim, B.; Durucan, S.; Wolf, K.-H.; Cai, W.; Agrawal, H.; Korre, A. Fracture behaviour and seismic response of naturally fractured coal subjected to true triaxial stresses and hydraulic fracturing. *Fuel* **2021**, *288*, 119618. [CrossRef]
22. Bai, M. Why are brittleness and fracability not equivalent in designing hydraulic fracturing in tight shale gas reservoirs. *Petroleum* **2016**, *2*, 1–19. [CrossRef]
23. Yan, C.; Zhao, Z.; Yang, Y.; Zheng, H. A three-dimensional thermal-hydro-mechanical coupling model for simulation of fracturing driven by multiphysics. *Comput. Geotech.* **2023**, *155*, 105162. [CrossRef]
24. Li, B.; Yu, H.; Xu, W.; Huang, H.; Huang, M.; Meng, S.; Liu, H.; Wu, H. A multi-physics coupled multi-scale transport model for CO2 sequestration and enhanced recovery in shale formation with fractal fracture networks. *Energy* **2023**, *284*, 129285. [CrossRef]
25. Zhang, D.; Zhang, L.; Tang, H.; Zhao, Y. Fully coupled fluid-solid productivity numerical simulation of multistage fractured horizontal well in tight oil reservoirs. *Pet. Explor. Dev.* **2022**, *49*, 382–393. [CrossRef]
26. Zhang, F.; Damjanac, B.; Maxwell, S. Investigating hydraulic fracturing complexity in naturally fractured rock masses using fully coupled multiscale numerical modeling. *Rock Mech. Rock Eng.* **2019**, *52*, 5137–5160. [CrossRef]
27. Liu, Y. On the displacement discontinuity method and the boundary element method for solving 3-D crack problems. *Eng. Fract. Mech.* **2016**, *164*, 35–45. [CrossRef]
28. Crouch, S.L. Solution of plane elasticity problems by the displacement discontinuity method. I. Infinite body solution. *Int. J. Numer. Methods Eng.* **1976**, *10*, 301–343. [CrossRef]
29. Liu, E.; Yao, T.; Qiao, L.; Li, J.; Wang, H.; Gao, Q. Research on the propagation mechanism of hydraulic fractures in infill horizontal wells. *Front. Earth Sci.* **2022**, *10*, 1026551. [CrossRef]
30. Zheng, P.; Xia, Y.; Yao, T.; Jiang, X.; Xiao, P.; He, Z.; Zhou, D. Formation mechanisms of hydraulic fracture network based on fracture interaction. *Energy* **2022**, *243*, 123057. [CrossRef]
31. Irwin, G.R. Analysis of stresses and strains near the end of a crack traversing a plate. *J. Appl. Mech.* **1957**, *24*, 361–364. [CrossRef]
32. Parker, A.P. *Stress Intensity Factors, Crack Profiles, and Fatigue Crack Growth Rates in Residual Stress Fields. Residual Stress Effects in Fatigue*; ASTM International: West Conshehoken, PA, USA, 1982.
33. Dumstorff, P.; Meschke, G. Crack propagation criteria in the framework of X-FEM-based structural analyses. *Int. J. Numer. Anal. Methods Geomech.* **2007**, *31*, 239–259. [CrossRef]